Supplement of Atmos. Chem. Phys., 26, 15423–15443, 2026
https://doi.org/10.5194/acp-26-15423-2026-supplement
© Author(s) 2026. CC BY 4.0 License.



Atmospheric Chemistry and Physics
Open Access

Supplement of

Retrieval of ultraviolet aerosol absorption from radiation measurements in young wildfire plumes

Jan-Lukas Tirpitz et al.

Correspondence to: Jan-Lukas Tirpitz (jltirpitz@gmail.com) and Jochen Stutz (jochen@atmos.ucla.edu)

The copyright of individual parts of the supplement might differ from the article licence.

S1 Measured particle size distributions and plume age dependence

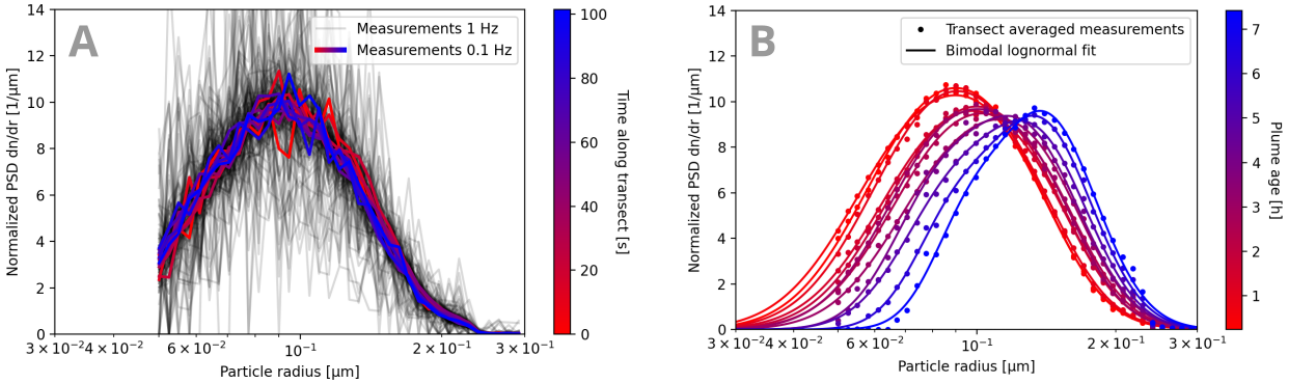


Figure S1. Measured particle size distributions from the Williams Flats fire. Panel A shows PSDs along Transect 3 for two temporal resolutions. The measurements reported at the original 1 Hz resolution exhibit significant noise. We calculated 10-second averages as a compromise between measurement noise and temporal resolution to investigate in-transect variability. The averages do not show significant variation. Panel B shows transect-averaged PSDs and corresponding bimodal fits (as described in Section 3.5 in the main text) for transects 1 (close to the fire) to 13 (far from the fire). They show particle growth with physical plume age (color coded).

S2 Sensitivity of aerosol optical properties to aerosol model simplifications

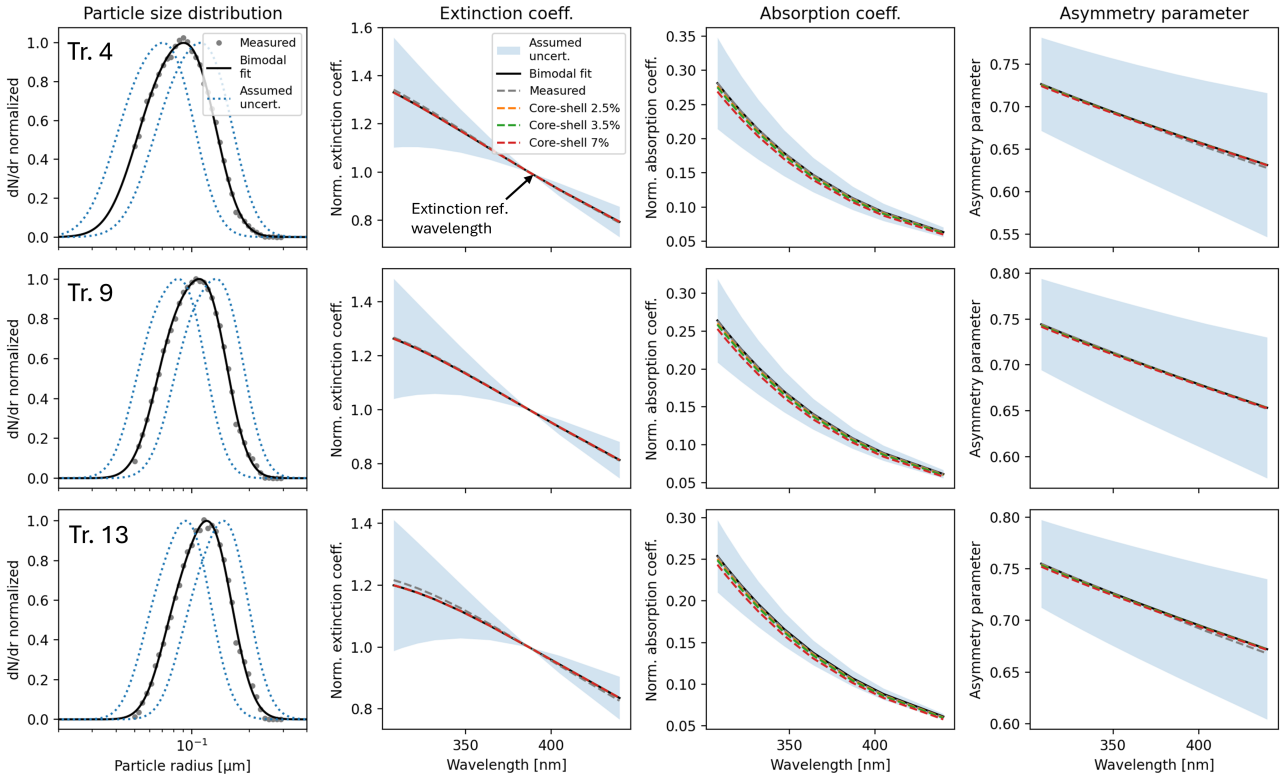


Figure S2. Sensitivity of calculated aerosol optical properties to two aerosol model simplifications: (1) the use of a bimodal PSD instead of the originally measured PSD and (2) NH_4NO_3 shells occupying 2.5%, 3.5%, and 7% of total dry particle volume (based on FIREX-AQ aerosol composition measurements; see main text Section 3.2). Panel rows show three Shady Fire plume transects (4, 9 and 13) representative for different plume ages. The first column of panels shows the originally measured PSDs from the laser aerosol spectrometer (grey dots), the bimodal fit used in the retrieval (black solid line), and the particle radius uncertainty assumed for our error propagation (blue dotted lines). The remaining panels show the optical properties (extinction coefficient, absorption coefficient and asymmetry parameter) for the measured PSD (grey dashed line), the bimodal fit (black solid line), core-shell configurations (colored dashed lines), and the assumed particle radius uncertainty (blue shaded region).

S3 Time series of individual retrievals for Lefthand and Williams Flats fires

Section 4.1 in the main text discusses the results of individual retrievals, but only shows data from the Shady fire (Figure 5 in the main text). This section provides similar figures for the Williams and the Lefthand fires (Figure S3 and Figure S4 respectively).

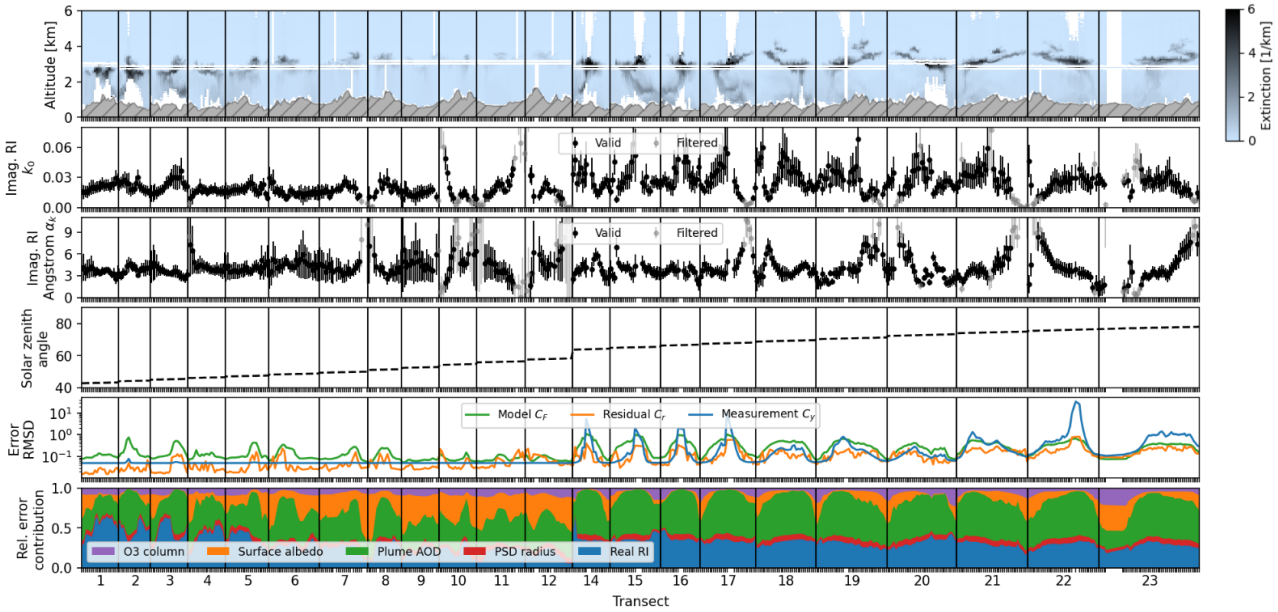


Figure S3. Results from retrievals performed on individual lidar profiles from transects of Williams Flats fire. Panel A shows the plume cross-sections as Lidar curtains of aerosol extinction coefficient. Panels B and C show the retrieval results of imaginary RI k_0 (at 387 nm) and angstrom coefficient α_k. Error bars indicate propagated uncertainties according to Eq. 11 in the main text. Grey data points are flagged as invalid according to the filter criteria described in Section 4.2 in the main text. Panel D shows solar zenith angle. Panel E indicates contributions of model error $\mathbf{C_F}$, fit residual $\mathbf{C_r}$ and measurement error $\mathbf{C_y}$ to the total retrieval uncertainty $\hat{\mathbf{C}}_\mathbf{x}$. Values represent RMSDs over the diagonal of the corresponding covariance matrix. Panel F illustrates the relative contributions of each critical fixed parameter to the total model covariance $\mathbf{C_F}$.

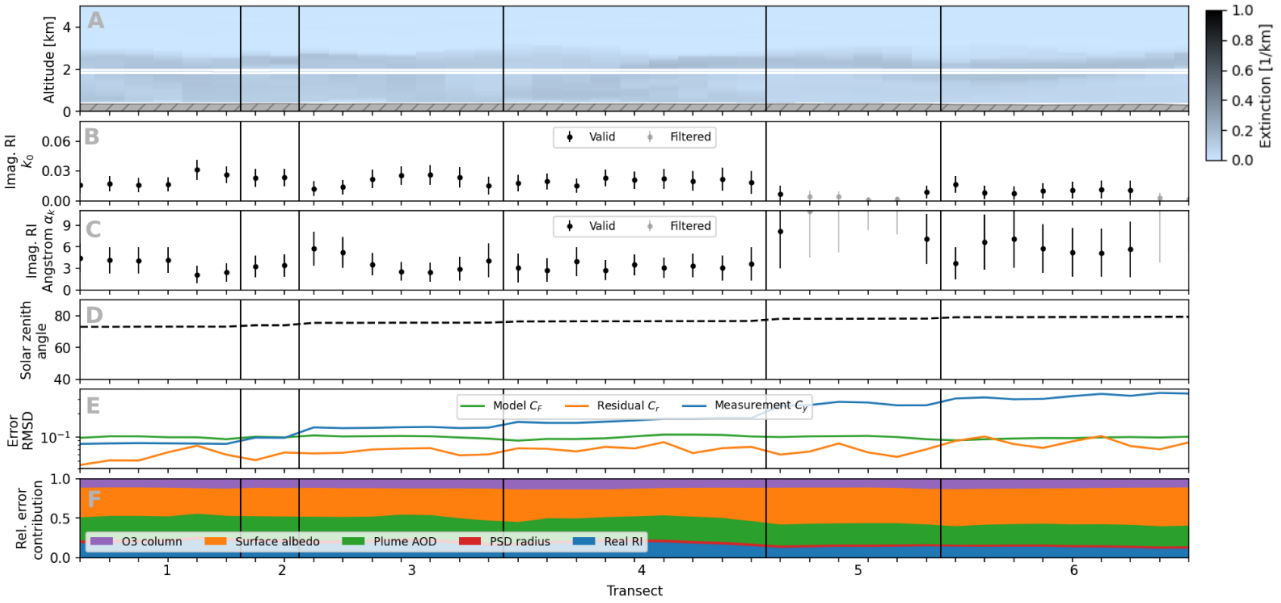


Figure S4. Results from retrievals performed for the Lefthand fire. See the Figure S3 caption for details.

S4 Determining the ideal retrieval conditions

The quality of the retrieval results depends on a number of factors (see Section 4.1 in main text for a detailed description). To determine the ideal retrieval conditions, we calculated errors of the retrieved parameters and the correlation between them for various synthetic scenarios reflecting typical conditions. The simulations assume a Gaussian-shaped BB plume with a vertical extent (full-width half-maximum) of 1 km and a center height of 2.5 km above the ground, which is at 2 km above sea-level (Figure S5). We used typical plume aerosol properties, based on FIREX-AQ measurements, literature values and retrieval results from this study. The SZA is assumed fixed to 30°. Uncertainties in the fixed critical model parameters are assumed to be 20 % on the PSD parameters, the real part of the refractive index, and the AOD and surface albedo, plus 5 % on the total ozone column.

We found that the most important factors controlling error levels are the flight altitude (with respect to the plume), and the plume AOD (Figure S5). Smallest retrieval errors and correlations were found when the aircraft is in the middle to upper part of the plume (Figure S5, A). In such cases the impact of uncertain assumptions on the surrounding environment is minimized. For instance, the impact of surface properties or background aerosols on the radiation field becomes small compared to the plume aerosol signal. At the same time, downwelling and upwelling radiation provide mostly independent information (downwelling radiation is dominated by direct beam attenuation; upwelling radiation includes an additional in-plume scattering event), maximizing the information content in the measurements. In terms of AOD, best results are achieved for AODs of 3 to 5 at 532 nm (Figure S5, B). For lower values of AOD, the aerosol signal decreases, while for high AOD, there is insufficient light reaching the instrument.

It should be noted that this analysis omits errors potentially arising from 3D radiative transfer effects. These can only be estimated using 3D RT models, which we considered to be out of the scope of the present study.

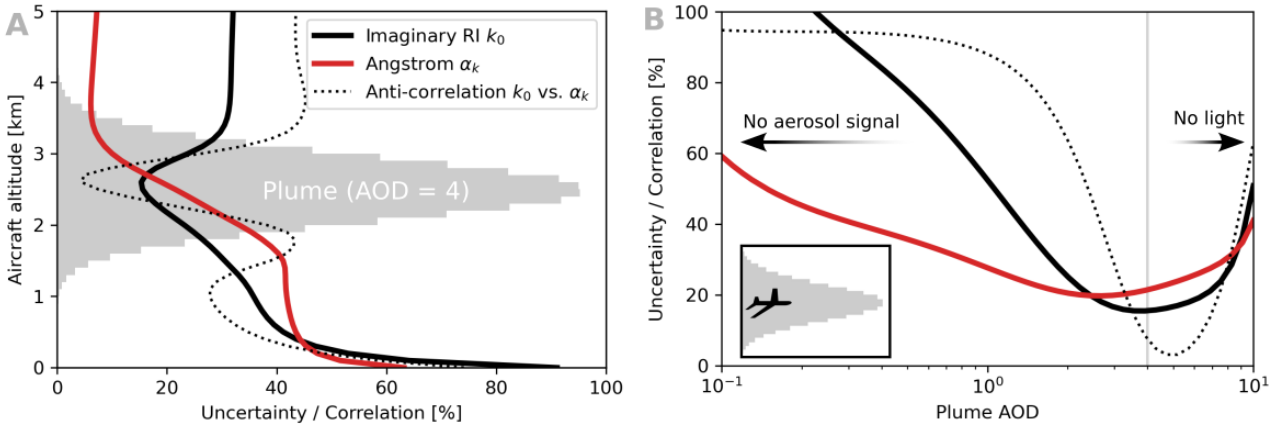


Figure S5. Errors and correlation for the retrieved parameters as functions of the flight altitude (panel A) and plume AOD (panel B). Simulations are based on synthetic scenarios with a Gaussian-shaped plume (see text). Panel B assumes the aircraft to be in the middle of the plume. All AODs are given for 532 nm.

S5 Individual retrieval results and transect averaging process

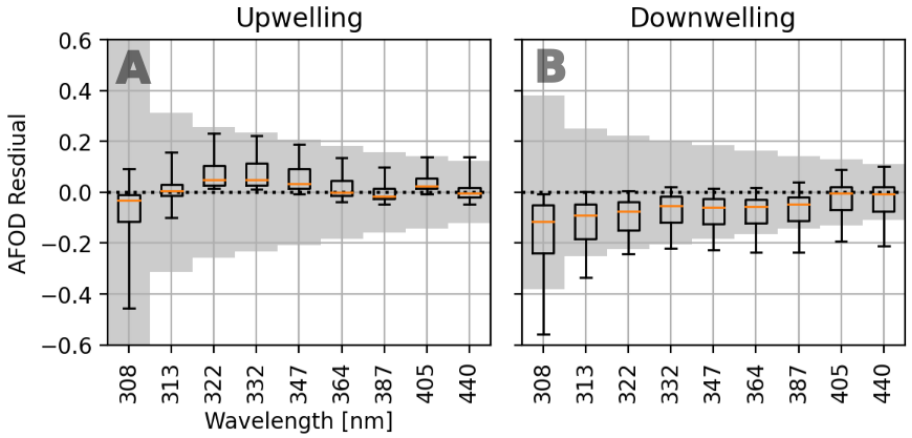


Figure S6. Statistics of the model-measurement residual in terms of AFOD (see main text Section 3.4). Orange lines indicate the median, boxes span the 25th to 75th percentile. Grey shaded areas indicate model and measurement errors ($\mathbf{S_F} + \mathbf{S_y}$).

Figure S7 illustrates the filtering and transect averaging process, providing a detailed view of retrieved imaginary RI, as well as derived VAC and SSA for two Shady fire transects. Transect 4 represents a particularly good case, with little variation among the individual retrievals (panel A). Transect 17 shows more retrieval instabilities and contains a number of individual retrieval results that were filtered out (dotted lines in panel C), as they did not satisfy the k_0/α_k criterion described in Section 4.2 in the main text. Such instability is likely due to 3D radiative effects, which are expected to appear more frequently here due to the high SZA (78°). Despite the different behavior of the individual retrievals, the resulting transect averages (panel B and D) agree well. Furthermore, the similar magnitudes of propagated uncertainties and scatter (RMSD) support the validity of our error propagation scheme.

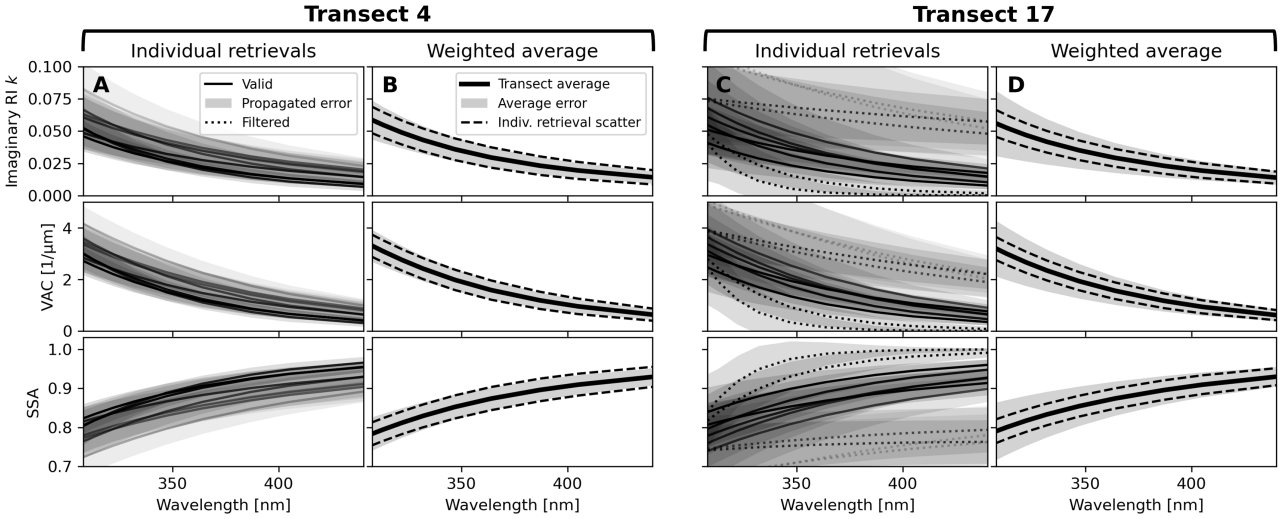


Figure S7. Spectrally resolved imaginary RI, volume absorption cross section (VAC), and single scattering albedo (SSA), for two transects from the Shady fire. Panel columns A and C show the results for the transect's individual retrievals. Transparency in the gray-shading indicates the level of uncertainty. Dotted lines indicate retrievals not satisfying the k_0/α_k filter criterion described in the main text. Panel columns B and D show error-weighted transect averages, where the dashed lines indicate the scatter (RMSD) between individual retrievals.

S6 Other complementary figures

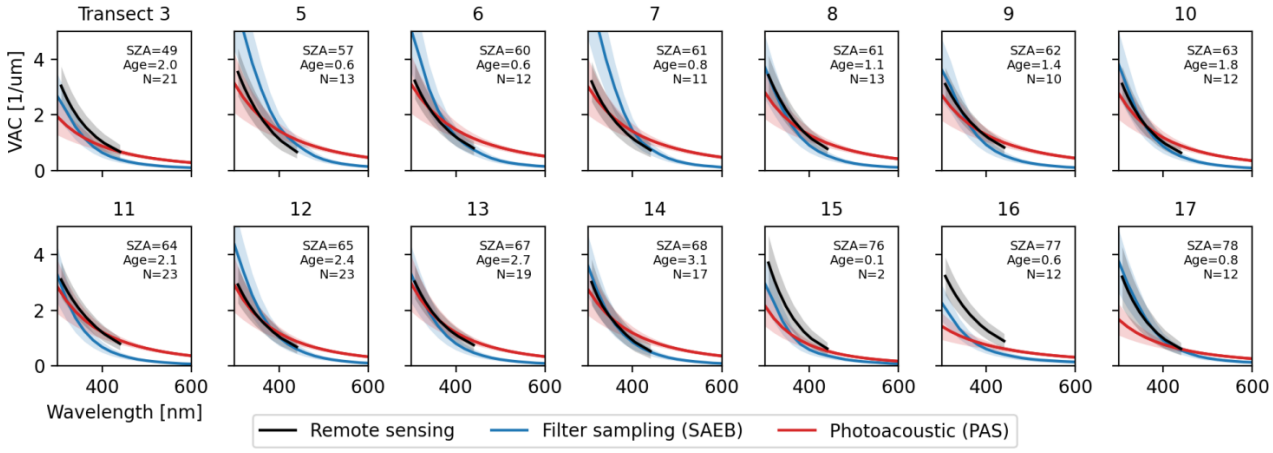


Figure S8. Supplement to figure 7 in the main text. While Figure 7 summarizes the comparison between different measurement techniques in a statistical boxplot, this figure shows the data for each transect. Inserts list the SZA in degrees, the plume age in hours, and the number of individual retrievals contributing to the transect.

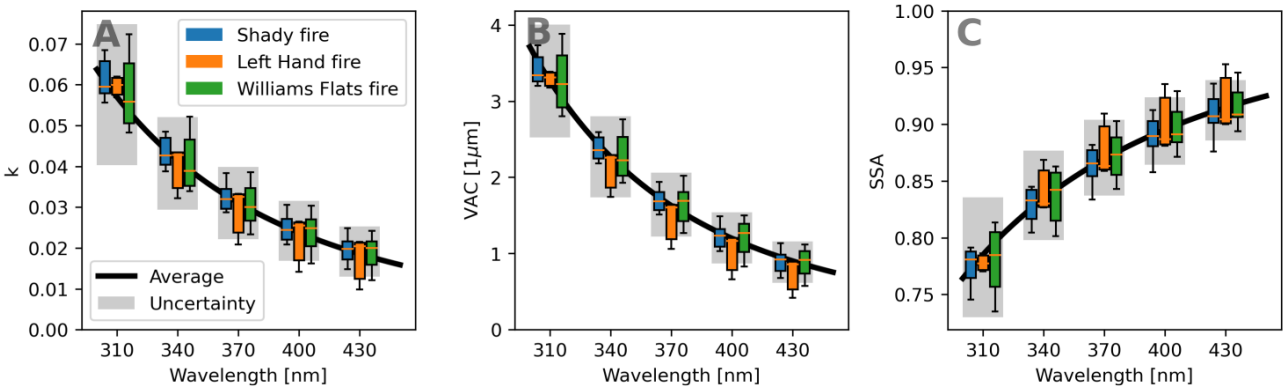


Figure S9. Same as Figure 9 in the main text but with relaxed settings for the filtering based on the k_0/α_k ratio, as described in Section 4.2. In Figure 9 we discarded retrieval results where k_0/α_k deviates from its median value by more than a factor of 5 or 0.2 in the upper or lower direction, respectively. Here, we allow for deviations by more than factors 10 and 0.1 respectively. The resulting increase in scatter and changes in the average results (compare figure 9) are negligible compared to the propagated uncertainties.

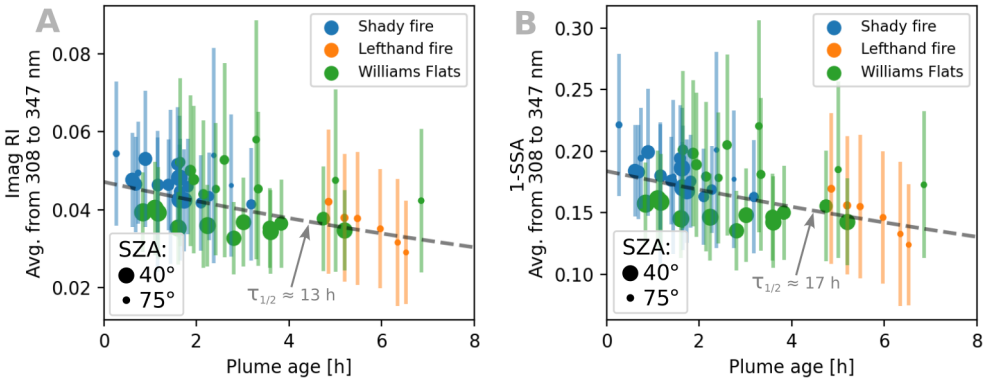


Figure S10. Dependence of imaginary RI (panel A) and 1-SSA (panel B) on plume age. Error bars represent propagated errors. Marker size indicates $\cos(\mathrm{SZA})$, as a proxy for the solar exposure. The grey dashed line shows an exponential fit, based on all data points.